BrainCSD: A Hierarchical Consistency-Driven MoE Foundation Model for Unified Connectome Synthesis and Multitask Brain Trait Prediction

Xiongri Shen, Jiaqi Wang, Yi Zhong, Zhenxi Song, Leilei Zhao, Liling Li, Yichen Wei, Lingyan Liang, Shuqiang Wang, Senior Member, Baiying Lei, Senior Member, Demao Deng, Zhiguo Zhang, Member

Abstract—Functional and structural connectivity (FC/SC) are key multimodal biomarkers for brain analysis, vet their clinical utility is hindered by costly acquisition, complex preprocessing, and frequent missing modalities. Existing foundation models either process single modalities or lack explicit mechanisms for cross-modal and cross-scale consistency. We propose BrainCSD, a hierarchical mixture-of-experts (MoE) foundation model that jointly synthesizes FC/SC biomarkers and supports downstream decoding tasks (diagnosis and prediction). BrainCSD features three neuroanatomically grounded components: (1) a ROIspecific MoE that aligns regional activations from canonical networks (e.g., DMN, FPN) with a global atlas via contrastive consistency; (2) a Encoding-Activation MOE that models dynamic cross-time/gradient dependencies in fMRI/dMRI; and (3) a network-aware refinement MoE that enforces structural priors and symmetry at individual and population levels. Evaluated on the datasets under complete and missing-modality settings, BrainCSD achieves SOTA results: 95.6% accuracy for MCI vs. CN classification without FC, low synthesis error (FC RMSE: 0.038; SC RMSE: 0.006), brain age prediction (MAE: 4.04 years), and MMSE score estimation (MAE: 1.72 points). Code is available in BrainCSD

Index Terms—foundation model, multitask brain trait prediction, brain connectome

I. INTRODUCTION

This research was supported by the National Natural Science Foundation of China (Grants 62306089, 32361143787, 82102032), the China Postdoctoral Science Foundation (Grants 2023M730873, GZB20230960), the key Project of Basic Research of Shenzhen (NO: JCYJ20200109113603854), and the Guangxi Natural Science Foundation (Grant No. 2023GXNS-FBA026073), the Shenzhen Science and Technology Program(Grant No. RCBS20231211090800003) (Corresponding authors: Zhenxi Song and Zhiguo Zhang.)

Xiongri Shen, Yi Zhong, Jiaqi Wang, Liling Li, and Leilei Zhao are with the Department of Computer Science and Technology, Harbin Institute of Technology, Shenzhen, 518055, China (email: xiongrishen@stu.hit.edu.cn, zoey24@stu.hit.edu.cn, 23b951063@stu.hit.edu.cn, 24S151033@stu.hit.edu.cn, 24b951025@stu.hit.edu.cn).

Zhenxi Song and Zhiguo Zhang is with School of Intelligence Science and Engineering, College of Artificial Intelligence, Harbin Institute of Technology, Shenzhen, Guangdong, China(e-mail: songzhenxi@hit.edu.cn, zhiguozhang@hit.edu.cn).

Baiying Lei is with School of Biomedical Engineering, National-Regional Key Technology Engineering Laboratory for Medical Ultrasound, Guangdong Key Laboratory for Biomedical, Measurements and Ultrasound Imaging, Shenzhen University Medical School, Shenzhen University, Shenzhen, China (e-mail: leiby@szu.edu.cn).

Shuqiang Wang is with the Shenzhen Institutes of Advanced Technology, Chinese Academy of Sciences, Shenzhen, China (e-mail: sq.wang@siat.ac.cn).

Demao Deng, Yichen Wei, and Lingyan Liangis with the Department of Radiology, The People's Hospital of Guangxi Zhuang Autonomous Region, Guangxi Academy of Medical Sciences. Nanning, China (email: demaodeng@163.com, 316644690@qq.com, lianglingyan163@126.com).

RALY and accurate diagnosis of neurodegenerative and neurodevelopmental disorders — including Alzheimer's disease (AD) [1]–[4], Parkinson's disease (PD) [5]–[9], and Autism Spectrum Disorder (ASD) [10]–[15] — is critical for timely intervention and improved long-term outcomes. Multimodal neuroimaging, particularly resting-state functional MRI (fMRI) and diffusion MRI (dMRI) [16], enables data-driven models. Recent work shows that *connectivity biomarkers* — functional connectivity (FC) and structural connectivity (SC) — offer superior discriminative power [17]. These quantify synchronized neural activity (FC) and anatomical white-matter wiring (SC) between regions of interest (ROIs), providing a systems-level view of brain dysfunction [18].

Yet two bottlenecks hinder clinical adoption. **First**, extracting FC/SC requires extensive preprocessing — slice-timing correction, motion realignment, co-registration, segmentation [19], brain extraction, eddy correction, tractography [20] — taking *months* per dataset. **Second**, real-world scans often lack fMRI/dMRI due to protocol limits or patient factors, leading to *incomplete connectivity profiles* and performance collapse.

Recent foundation models have improved diagnostic generalizability. **BrainLM** [21] introduced masked self-supervision for intra-modality tasks (e.g., age prediction). **BrainSN** [22] used ROI masking + Transformer for ASD/ADHD. **Brain-Mass** [23] built a biomarker-level model using atlas priors, covering AD/PD/ADHD. Yet none address missing-modality robustness — a critical gap for real-world deployment.

The Mixture-of-Experts (MoE) architecture has emerged as a key enabler for scaling foundation models [24], especially when combined with Transformers. Yet, current MoE research remains narrowly focused on improving gating mechanisms or router designs [25] — largely ignoring *domain-specific structural priors*. This is particularly limiting in diagnostics, where expert specialization should be guided by biologically meaningful units, not just data-driven routing signals.

Although prior foundation models have embedded anatomical or functional priors into Transformer layers, no existing MoE explicitly structures expert routing around neuroanatomically defined brain networks — such as the Cerebellar Network (CER), Cingulo-Opercular Network (CON), Default Mode Network (DMN), Occipital Network (OCC), Frontoparietal Network (FPN), and Sensorimotor Network (SEN) — which are well-established as pathophysiologically critical in neurological and neurodevelopmental disorders [18], [26], [27]. This gap leaves MoE models biologically ungrounded

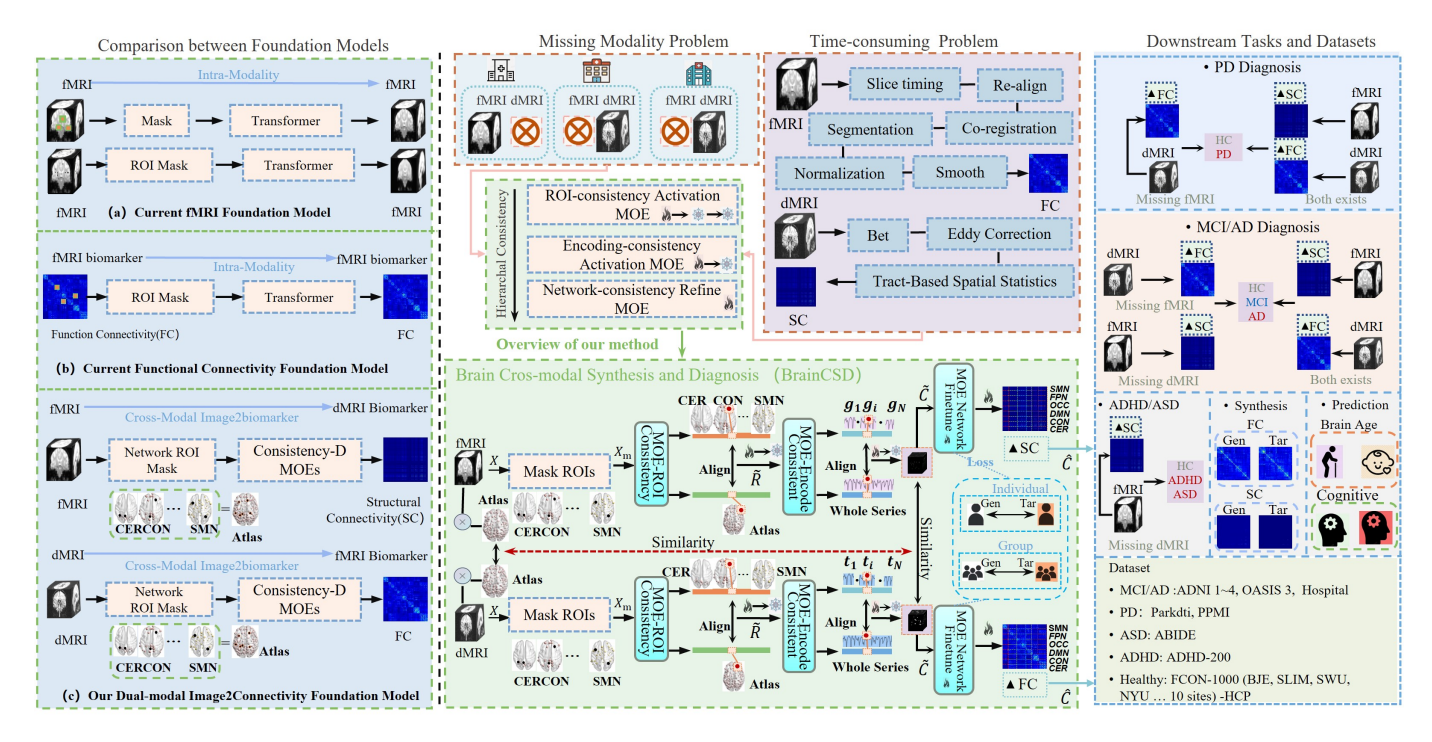


Fig. 1: Hierarchical consistency-driven (consistency-D) MoE for connectome synthesis and prediction under missing modalities, via ROI (Network \leftrightarrow Atlas) \rightarrow Encoding (time[t]/gradient [g] point \leftrightarrow Whole series) \rightarrow Neuroanatomy-informed MOE.

and limits their interpretability, generalizability, and clinical utility — a limitation BrainCSD directly addresses through activation-consistency-driven, network-aligned expert routing.

We propose **BrainCSD** — **Brain** Connectivity Synthesis and **Decode** — an **Hierarchical Consistency-Driven MOE Foundation Model** for joint medical image biomarker synthesis and decode. BrainCSD synthesizes FC/SC directly from raw fMRI/dMRI — bypassing preprocessing — and enables robust diagnosis even when one modality is missing.

Our hierarchical consistency-driven MoE enforces biological plausibility across three stages: (1) ROI-consistency Activation MoE — activates disease-relevant ROIs via atlas-MOEs and network-MOEs alignment; (2) Encoding Activation MoE — treats each dual-modal neuro-imaging encoding-point as an expert to model dynamic FC/SC with temporal/gradient consistency between whole series MOEs; (3) Network-Aware MoE Finetuning — refines connectivity using individual and group structural constraints (symmetry, sparsity, para-graphics consistency).

Contributions:

- We propose the hierarchical MoE foundation model that explicitly aligns expert routing with canonical brain networks (DMN, FPN, CON, etc.) through activation-consistency constraints across ROI, encoding, and population levels.
- 2) We demonstrate that BrainCSD can synthesize diagnostically usable FC/SC from a single modality (e.g., dMRI-only), enabling MCI diagnosis with 95.6% accuracy—outperforming real FC-based models in missing-modality settings.
- 3) We validate robustness across 7K+ subjects, 22 sites, 15 tasks, 9 datasets, and 5 disorders, showing <5% performance variance across age, sex, and cognitive subgroups

— a critical step toward clinical deployment.

II. RELATED WORK

Connectivity Biomarkers for Diagnosis. Functional (FC) and structural connectivity (SC) biomarkers offer superior generalizability and neurobiological interpretability over raw imaging features [1], [2], [5]. Disruptions in canonical networks (e.g., DMN, FPN) correlate strongly with disorders like AD, PD, and ASD [10], [12], [13], capturing systems-level pathology that enhances cross-dataset robustness.

Limitations of Neuroimaging Foundation Models. Current foundation models (e.g., BrainLM [21], BrainSN [22], BrainMASS [23]) fall into *image-level* or *biomarker-level* categories. While biomarker-level models show stronger diagnostic transferability, they do not explicitly model robustness to missing modalities or eliminate dependency on slow, preprocessing-heavy pipelines, two critical requirements for real-world deployment that BrainCSD addresses by directly synthesizing FC/SC from uni-modality inputs.

MoE with Neuroscientific Priors. MoE architectures excel in scalable representation learning [24], [25], yet generic routing mechanisms (e.g., top-k, attention-gating) often overlook domain-specific structure. As BrainMASS demonstrates, embedding neuroanatomical priors (e.g., atlas-based positional embeddings) improves performance. BrainCSD advances this by explicitly aligning MoE expert routing with canonical brain networks (DMN, FPN, CON, etc.) and temporal/gradient dynamics — ensuring that each expert specializes in a biologically meaningful subsystem.

Synthesis Without Diagnostic Validation. Existing FC/SC synthesis methods, based on GANs, diffusion models, or VAEs [28]–[32] — primarily optimize statistical or visual

TABLE I: Summary of Datasets Used in the Study

Stage	Dataset	Sites	Modality	Participants	F/M	Age	MMSE/MoCA	Disease (nums)
	ADNI 1-4	ADNI 1-4	fMRI-dMRI	894	430/464	64.48 ± 5.73	29.55 ± 0.72	HC(468)/MCI(370)/AD(56)
	OASIS-3	OASIS-3	fMRI-dMRI	1809	905/904	68.62 ± 4.73	28.90 ± 1.09	HC(1315)/MCI(229)/AD(265)
	Hospital	Hospital	fMRI-dMRI	254	114/140	64.70 ± 6.47	29.00 ± 1.41	HC(77)/MCI(177)
ROI/Encode	-	BIE, SLIM, SWU, HNU, BNU,						
activation	FCON-1000	IPCAS, MRN, NKI, NYU,	fMRI-dMRI	1705	853/852	24.30 ± 2.37	/	HC(1705)
activation		SWU, XHCUMS						
	Park-dti	Park-dti	dMRI	53	25/28	64.80 ± 7.44	28.10 ± 1.63	HC(26)/PD(27)
	PPMI	PPMI	fMRI-dMRI	138	54/94	64.75 ± 8.78	/	HC(18)/PD(120)
	ABIDE	ABIDE	fMRI	1073	149/924	16.60 ± 8.08	/	HC(558)/ASD(515)
	HCP	HCP	fMRI-dMRI	1207	656/551	27.5 ± 2.94	/	HC(1207)
	ADHD-200	ADHD-200	fMRI	194	49/145	11.4 ± 8.38	/	HC(27)/167
Finetune-FC	ADNI, FCON-1000, Hospital	ADNI, FCON-1000, Hospital	fMRI-dMRI	1277	/	/	/	/
Finetune-SC	ADNI	ADNI	fMRI-dMRI	269	/	/	/	/

TABLE II: Overview of downstream tasks and datasets.

Scenario	Task	Dataset	Mod.	Subj.
Diagnosis				
Missing fMRI	MCI	ADNI 1-4	dMRI	269
Wiissing iiviiki	PD	Park-dti	dMRI	53
Missing	MCI	ADNI 1-4, Hospital, FCON-1000	fMRI	1277
dMRI	ASD	ABIDE	fMRI	1073
	ADHD	ADHD-200	fMRI	194
Dual-modal	AD	ADNI 1-4, OASIS-3, Hospital,	f+D	4934
Missing		HCP, FCON-1000		
_	PD	PPMI	f+D	138
Prediction				
Dual Modal	Age (w/ sub)	ADNI 1-4, OASIS-3, Hospital,	f+D	4934
Missing		PPMI, HCP, FCON-1000		
· ·	MMSE (w/ sub)	ADNI 1-4, OASIS-3, Hospital	f+D	2957
Synthesis				
Missing dMRI	FC (w/ sub)	ADNI 1-4, Hospital, FCON-1000	fMRI	1277
Missing fMRI	SC (w/ sub)	ADNI 1-4	dMRI	269

Note: ADHD = Attention Deficit Hyperactivity Disorder; MMSE = Mini-Mental State Examination: f+D = fMRI + dMRI: (w/ sub) = with subgroup stratification.

fidelity. Few validate whether synthesized biomarkers preserve diagnostic signal, and even fewer evaluate under missingmodality settings. BrainCSD bridges this gap by jointly optimizing synthesis quality and downstream tasks across complete and incomplete data regimes.

III. METHODS

We present **BrainCSD**, a MoE framework for synthesizing functional and structural connectomes (FC/SC) from restingstate fMRI and diffusion MRI (dMRI). As illustrated in Fig. 2, BrainCSD comprises three synergistic stages: (1) ROI Activation MoE for spatial region selection grounded in neuroanatomical priors, (2) Encode Dynamics MoE for modeling encoding-varying (time/gradient) brain states with a fixed set of encode experts, and (3) Network-Aware MoE Finetuning for refining connectivity matrices with structural symmetry and network constraints. This hierarchical design enables precise, interpretable, and biologically plausible connectome synthesis.

A. ROI Activation MoE

Motivation. Neuroimaging data contains abundant noninformative background voxels and anatomically irrelevant regions. To focus on disease-diagnostic signals, we design a hierarchical MoE structure that first isolates brain tissue, then activates canonical networks (e.g., DMN, FPN), and finally enforces consistency between network-wise and whole-atlas selections via contrastive learning.

Network-Level Masking. Let $\mathbf{X}_f \in \mathbb{R}^{T \times V}$ and $\mathbf{X}_d \in \mathbb{R}^{G \times V}$ denote the fMRI encoding series and dMRI-derived gradient encoding seires, respectively, where T/G is the number of time/gradient points and V is the number of ROIs. Based on a standard brain atlas partitioned into six canonical networks — Cerebellar (CER), Cingulo-Opercular (CON), Default Mode (DMN), Occipital (OCC), Frontoparietal (FPN), and Somatomotor (SEN) — we define binary masks $\mathbb{M}_n \in \{0,1\}^V$ for each network n. The masked input is as:

$$\mathbf{X}_m = \mathbf{X} \odot \left(\sum_{n=1}^6 \mathbb{M}_n \right), \tag{1}$$

where \odot denotes element-wise multiplication, and X represents either \mathbf{X}_f or \mathbf{X}_d .

Tissue-Level MoE. To suppress non-brain background, we apply a Transformer encoder followed by a Tissue MoE $\mathcal{T}=$ $\{\mathcal{T}_1, \dots, \mathcal{T}_K\}$ with gating function $g_{\mathcal{T}}(\mathbf{Z}) = \operatorname{softmax}(\mathbf{W}_a \mathbf{Z})$. The embedding is:

$$\mathbf{Z}_{t} = \sum_{i \in \text{Top-1}(g_{\mathcal{T}}(\mathbf{Z}))} \left[g_{\mathcal{T}}(\mathbf{Z})_{i} \cdot \mathcal{T}_{i}(\mathbf{Z}) \right], \tag{2}$$

where $\mathbf{Z} = \operatorname{Transformer}(\mathbf{X}_m)$ is the initial embedded representation.

Network-Level MoE. For each neuro-anatomical network $\mathcal{N} \in \{\mathcal{D}, \mathcal{F}, \mathcal{C}, \mathcal{S}, \mathcal{E}, \mathcal{O}\}$ (corresponding to DMN, FPN, etc.), we define a network-specific MoE $\mathcal{N}^r = \{\mathcal{N}_1^r, \dots, \mathcal{N}_k^r\}$ with gating $g_{\mathcal{N}^r}$. The activated representation per network is:

$$\mathbf{Z}_{\mathcal{N}^r} = \sum_{j \in \text{Top-1}(g_{\mathcal{N}^r}(\mathbf{Z}_t))} \left[g_{\mathcal{N}^r}(\mathbf{Z}_t)_j \cdot \mathcal{N}_j^r(\mathbf{Z}_t) \right].$$
 (3)

Global Consistency via Contrastive Learning. To align network-wise and atlas-wise activations, we introduce a global router \mathcal{G} and an atlas-level MoE \mathcal{A} . Let \mathbf{Z}_G = $\mathcal{G}(\operatorname{Concat}(\{\mathbf{Z}_{\mathcal{N}^r}\}))$ and $\mathbf{Z}_A = \mathcal{A}(\mathbf{Z}_t)$. We enforce consistency by applying tissue filtering again:

$$\mathbf{Z}_{tG} = \sum_{l \in \text{Top-1}(g_{\mathcal{T}}(\mathbf{Z}_G))} [g_{\mathcal{T}}(\mathbf{Z}_G)_l \cdot \mathcal{T}_l(\mathbf{Z}_G)], \qquad (4)$$

$$\mathbf{Z}_{tG} = \sum_{l \in \text{Top-1}(g_{\mathcal{T}}(\mathbf{Z}_G))} [g_{\mathcal{T}}(\mathbf{Z}_G)_l \cdot \mathcal{T}_l(\mathbf{Z}_G)], \qquad (4)$$

$$\mathbf{Z}_{tA} = \sum_{o \in \text{Top-1}(g_{\mathcal{T}}(\mathbf{Z}_A))} [g_{\mathcal{T}}(\mathbf{Z}_A)_o \cdot \mathcal{T}_o(\mathbf{Z}_A)]. \qquad (5)$$

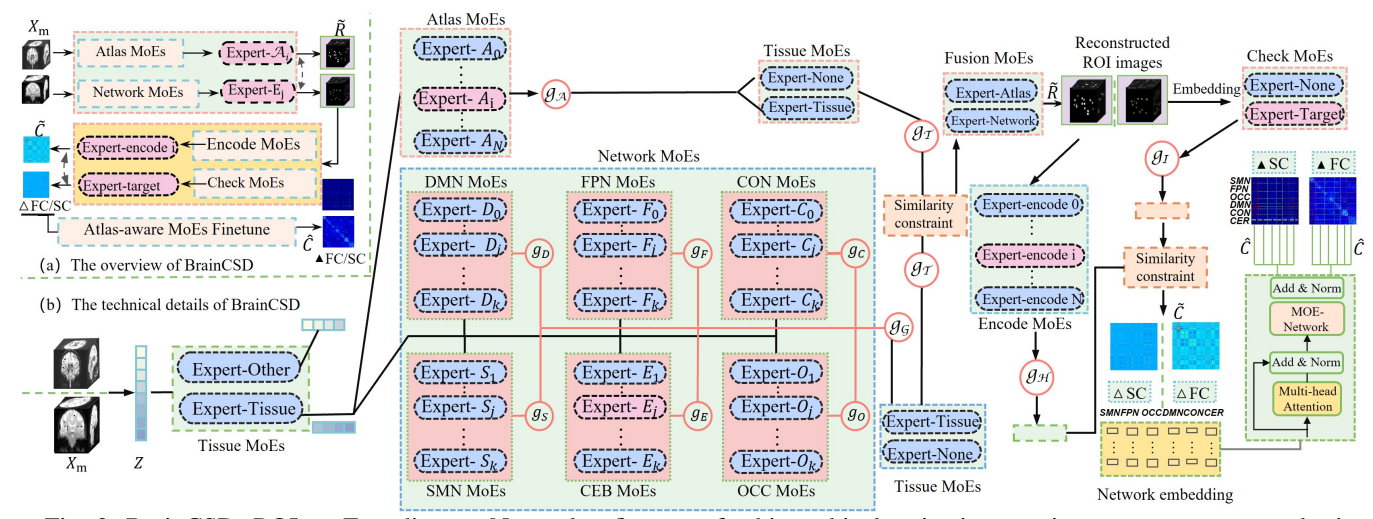


Fig. 2: BrainCSD: ROI → Encoding → Network refinement for hierarchical activation-consistent connectome synthesis

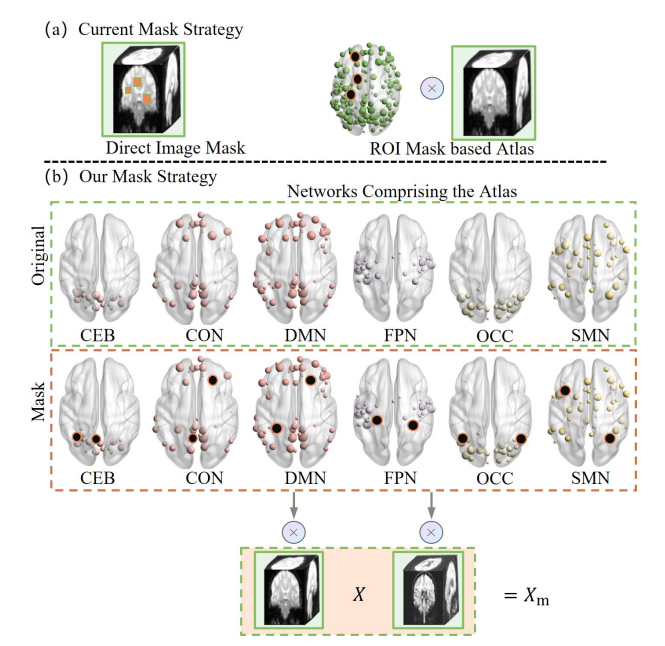


Fig. 3: **Network-Level Masking Strategy.** Regions from six canonical networks are selectively masked during training to enforce region-specific feature learning.

A contrastive loss aligns these representations within a batch of K subjects:

$$\mathcal{L}_{\text{cont}} = -\log \frac{\exp(s(\mathbf{Z}_{tA}, \mathbf{Z}_{tG})/\tau)}{\sum_{k=1}^{K} \exp\left(s(\mathbf{Z}_{tA}, \mathbf{Z}_{tG}^{(k)})/\tau\right)},$$
 (6)

where $s(\mathbf{u},\mathbf{v}) = \frac{\mathbf{u}^{\top}\mathbf{v}}{\|\mathbf{u}\|\|\mathbf{v}\|}$ is cosine similarity and τ is a temperature hyperparameter.

Reconstruction to Imaging Space. The fused $\mathbf{Z}_f = \operatorname{Concat}(\mathbf{Z}_G, \mathbf{Z}_A)$ is decoded by a full-capacity MoE \mathcal{R} (i.e., all experts contribute) to reconstruct ROI encoding series. The output is reshaped and positional encoding is removed to yield $\mathbf{R} \in \mathbb{R}^{E \times V}$:

$$\widetilde{\mathbf{R}} = \operatorname{Reshape}\left(\operatorname{MLP}\left(\mathbf{Z}_f\right)\right) \in \mathbb{R}^{E \times V},$$
 (7)

where E = T/V. The final ROI response is reconstructed by removing positional encoding:

$$\widetilde{\mathbf{R}} = \mathbf{Z}_f - \mathbf{E}_{\text{pos}}.$$
 (8)

B. Encoding Activation MoE

Motivation. The connectivity is inherently dynamic — static ROI representations fail to capture encode evolution critical for accurate FC/SC estimation. We model encode dynamics (time axis in fMRI and gradient axis in dMRI) via a MoE with *K* encode experts, each capturing a distinct phase of brain state evolution.

Given the ROI response $\widetilde{\mathbf{R}} \in \mathbb{R}^{E \times V}$, E denotes encoding-vary point, we first embed it via Transformer to obtain $\mathbf{Z}_{\widetilde{\mathbf{R}}} \in \mathbb{R}^{E \times D}$. A Encoding Activation MoE $\mathcal{H} = \{\mathcal{H}_1, \dots, \mathcal{H}_T\}$ with gating $g_{\mathcal{H}}$ computes:

$$\mathbf{Z}_{E} = \sum_{k=1}^{K} g_{\mathcal{H}}(\mathbf{Z}_{\widetilde{\mathbf{R}}})_{k} \cdot \mathcal{H}_{k}(\mathbf{Z}_{\widetilde{\mathbf{R}}})$$
(9)

Then a check MOE \mathcal{I} with gating $g_{\mathcal{I}}$ is used to embed the whose series:

$$\mathbf{Z}_{I} = \sum_{p \in \text{Top-1}(g_{\mathcal{I}}(\mathbf{Z}_{\widetilde{\mathbf{R}}}))} \left[g_{\mathcal{I}}(\mathbf{Z}_{\widetilde{\mathbf{R}}}) \cdot \mathcal{I}_{p}(\mathbf{Z}_{\widetilde{\mathbf{R}}}) \right], \quad (10)$$

To ensure encode stability, we apply a symmetric encode consistency loss:

$$\mathcal{L}_{\text{en}} = \|\mathbf{Z}_E - \mathbf{Z}_I\|_F^2. \tag{11}$$

The encoding-consistent ROI response $X_T = Z_E - E_{pos}$ is used to compute preliminary FC/SC matrices:

$$\widetilde{\mathbf{C}} = \operatorname{Corr}(\mathbf{X}_T),$$
 (12)

where $Corr(\cdot)$ computes Pearson correlation for FC or streamline counts for SC.

C. Network-Aware MoE Finetuning

Motivation. Raw synthesized connectivity matrices often lack neurobiological plausibility — e.g., broken symmetry, unrealistic sparsity, or misaligned network boundaries. We introduce

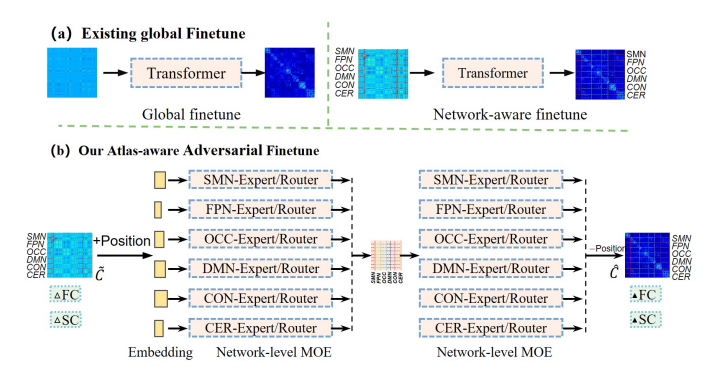


Fig. 4: **Network-Aware Finetuning.** Each network is refined by a dedicated MoE expert, ensuring anatomical and diagnostic consistency.

a finetuning stage that refines $\widetilde{\mathbf{C}}$ using network-constrained MoEs and structural priors. We vectorized $\widetilde{\mathbf{C}} \in \mathbb{R}^{V \times V}$ into $c \in \mathbb{R}^{V^2}$ and apply a linear projection before Transformer.

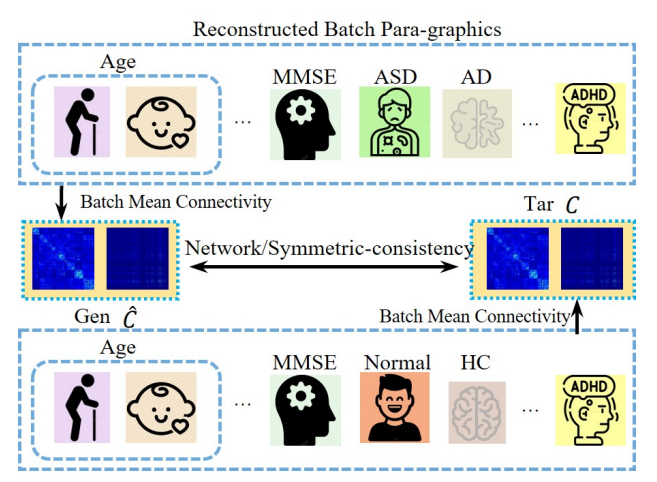
Let $\mathbf{Z}_C = \operatorname{Transformer}(\widetilde{\mathbf{C}})$. For each network $\mathcal{N}^f \in \{\mathcal{D}^f, \mathcal{F}^f, \dots, \mathcal{O}^f\}$, we apply a finetuning MoE:

$$\mathbf{Z}_{\mathcal{N}^f} = \sum_{j \in \text{Top-1}(g_{\mathcal{N}^f}(\mathbf{Z}_C))} \left[g_{\mathcal{N}^f}(\mathbf{Z}_C)_j \cdot \mathcal{N}_j^f(\mathbf{Z}_C) \right]. \quad (13)$$

The refined connectivity $\hat{\mathbf{C}}$ is obtained by inverse embedding and enforces symmetry:

$$\hat{\mathbf{C}} = \mathrm{MLP}(\mathrm{Concat}(\{\mathbf{Z}_{\mathcal{N}^f}\})) - \mathbf{E}_{\mathrm{pos}}, \quad \hat{\mathbf{C}} \leftarrow \frac{\hat{\mathbf{C}} + \hat{\mathbf{C}}^\top}{2}.$$
(14)

D. Loss Functions



Target Batch Para-graphics

Fig. 5: **Group-Level Consistency.** Connectivity features are regularized to be consistent within clinical/demographic subgroups, enhancing diagnostic utility.

Reconstruction Loss. At ROI and Encoding stages, we use mean squared error (MSE) and contrastive loss to reconstruct ROIs end encoding seiries, the R is generated by apply the atlas to X, i denotes f/d modality:

$$\mathcal{L}_{\text{cont_e}} = \|\mathbf{R} - \hat{\mathbf{R}}\|_F^2 + \|c(\mathbf{R}_1, \mathbf{R}_2) - c(\hat{\mathbf{R}}_1, \hat{\mathbf{R}}_2)\|_F^2, \quad (15)$$

where c is the contrastive loss function defined as:

$$c(\mathbf{u}, \mathbf{v}) = -\log \frac{\exp(s(\mathbf{u}, \mathbf{v})/\tau)}{\sum_{k=1}^{K} \exp(s(\mathbf{u}, \mathbf{v})/\tau)},$$
 (16)

with $s(\mathbf{u}, \mathbf{v}) = \frac{\mathbf{u}^{\top} \mathbf{v}}{\|\mathbf{u}\| \|\mathbf{v}\|}$ being the cosine similarity and τ being a temperature hyperparameter.

$$\mathcal{L}_{\text{sym}} = \|\hat{\mathbf{C}} - \hat{\mathbf{C}}^{\top}\|_F^2, \tag{17}$$

$$\mathcal{L}_{\text{conn}} = \|\mathbf{C} - \hat{\mathbf{C}}\|_F^2 + \lambda \mathcal{L}_{\text{sym}}, \tag{18}$$

where λ is a balancing hyperparameter.

Group-Level Consistency (Optional). To leverage population-level patterns, we optionally minimize variance of connectivity features within demographic/clinical subgroups (e.g., diagnosis, age):

$$\mathcal{L}_{\text{group}} = \mathbb{E}_{s \in \mathcal{S}} \left[\text{Var}_{q \in s} \left(\phi(\hat{\mathbf{C}}_q) \right) \right], \tag{19}$$

where S is the set of subgroups and $\phi(\cdot)$ is a feature extractor (e.g., network strength).

IV. EXPERIMENT

A. Datasets and Downstream Evaluation

We evaluate **BrainCSD** on a multi-site neuroimaging cohort detailed in Table **I**, which includes ADNI, OASIS-3, and the Human Connectome Project (HCP), with annotations for modality (fMRI, dMRI), demographics (age, sex), cognitive scores (MMSE/MoCA), and clinical diagnoses (e.g., Alzheimer's disease, Parkinson's disease, autism spectrum disorder, and healthy controls). Downstream tasks—spanning disease classification, cognitive score regression, and connectome synthesis—are defined in Table II. To ensure statistical robustness and mitigate site/scanner bias, all tasks employ **5fold stratified cross-validation** with an 8:1:1 subject-level split for training, validation, and testing, following established protocols in foundational neuroimaging AI [22], [23].

B. Implementation Details

Our model is trained end-to-end across three stages—*ROI Activation, Encoding Activation*, and *Network-Aware Finetuning* (Sec. III), implemented in PyTorch with AdamW (lr=1e⁻⁴, weight decay=1e⁻²), mixed-precision training, and gradient clipping (max norm=1.0). Pretraining runs for 1000 epochs with early stopping; finetuning for 300 epochs.

- a) Stage 1: ROI Activation.: We use a 4-layer Transformer encoder-decoder (hidden dim: 512, 8 heads, learnable positional encoding shared across modalities) to ensure invertible latent projection. All MoEs employ **Top-1 gating** for sparsity and interpretability:
- Atlas MoE (A): 160 experts aligned with Dosenbach160 atlas [33].
- Network MoEs (D, F, C, S, E, O): Expert counts (18, 32, 34, 22, 21, 33) reflect network size and functional complexity (e.g., DMN > OCC).
- Tissue MoE (T): 2 experts (Tissue/Other) for modalityspecific routing.

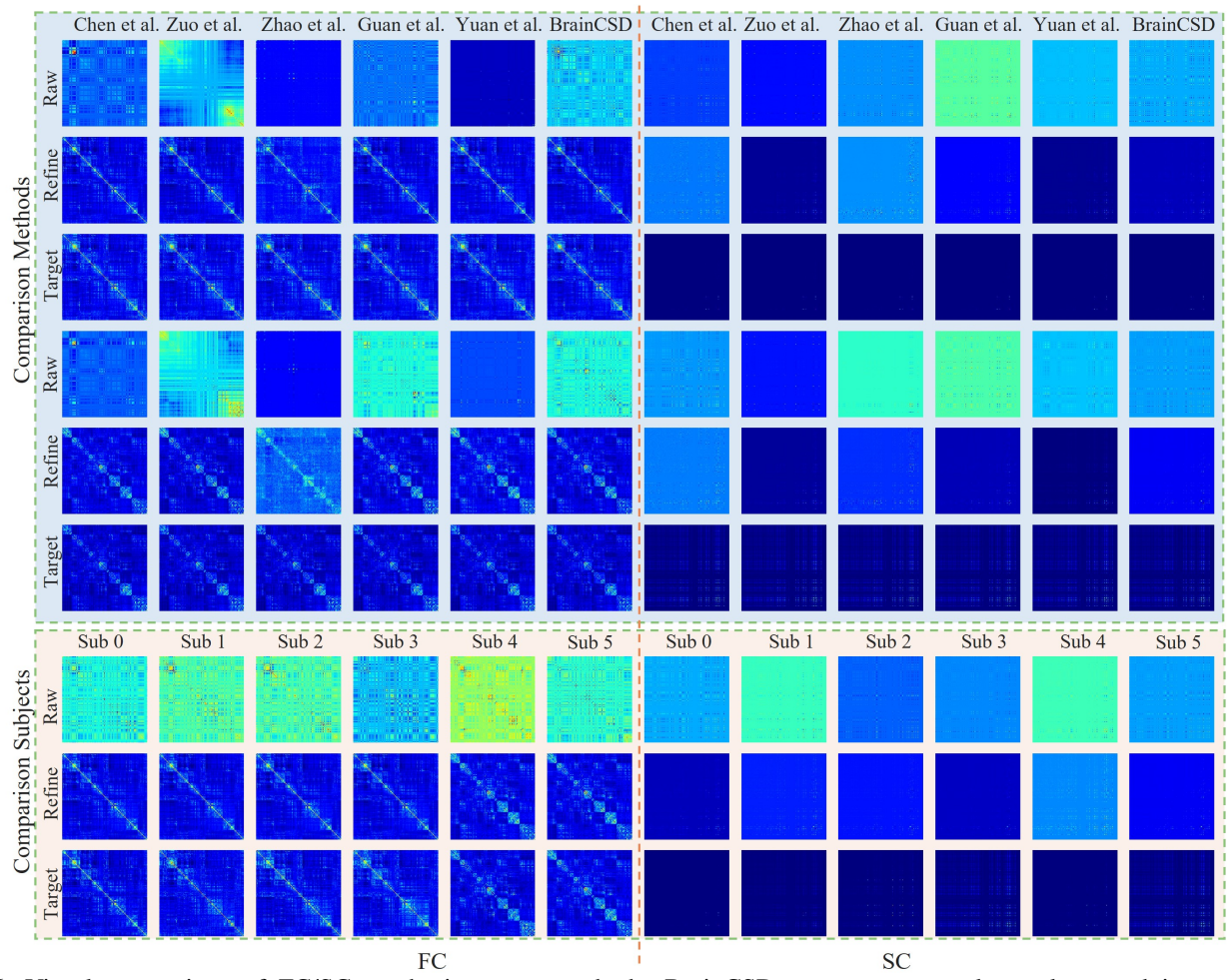


Fig. 6: Visual comparison of FC/SC synthesis across methods. BrainCSD preserves network topology and inter-regional correlations, while baselines exhibit blurring or anatomical misalignment.

- Fusion MoE (G): 6 experts (one per canonical network) for dynamic interaction selection.
- Reconstruction MoE (R): 2 experts with dense gating to ensure full gradient flow during pretraining.

Contrastive loss \mathcal{L}_{cont} (Eq. 6) uses temperature $\tau = 0.07$.

- b) Stage 2: Encoding Activation.: To model dynamic functional connectivity without inductive bias, we deploy:
- Encode MoE (\mathcal{H}): 200 experts (T/G=200), Top-1 gated.
- Encode Consistency MoE: Mirrors \mathcal{H} and enforces smoothness via $\mathcal{L}_{\mathrm{en}} = \|\mathbf{Z}_E \mathbf{Z}_I\|_F^2$.

This dual-MoE design addresses *temporal/gradient sparsity* in static FC/SC models [34], avoiding RNNs or convolutions to let MoEs learn dynamics data-drivenly, resulting better biomarker (FC/SC) modeling performance.

c) Stage 3: Network-Aware Finetuning.: Preliminary connectomes $\tilde{\mathbf{C}}$ are refined using network-specific MoEs $(\mathcal{D}^f, \mathcal{F}^f, \dots, \mathcal{O}^f)$ with expert counts matching Stage 1. We enforce symmetry via $\hat{\mathbf{C}} \leftarrow (\hat{\mathbf{C}} + \hat{\mathbf{C}}^\top)/2$ and minimize

$$\mathcal{L}_{\mathrm{conn}} = \|\mathbf{C} - \hat{\mathbf{C}}\|_F^2 + \lambda \|\hat{\mathbf{C}} - \hat{\mathbf{C}}^\top\|_F^2, \quad \lambda = 0.5.$$

Optionally, group-level consistency loss $\mathcal{L}_{\mathrm{group}}$ (Eq. 19) enhances diagnostic separability (e.g., minimizing intra-class variance for AD vs. HC).

- d) Why This Design?:
- Top-1 gating mirrors neurobiological sparsity—cortical columns activate selectively [35].
- Expert counts are neuroanatomically grounded: proportional to ROI count (160), network complexity (DMN > OCC), and tissue dichotomy (Tissue/Other).
- Dense gating in \mathcal{R} ensures stable gradient flow during self-supervised pretraining.
- **No recurrence**: Unlike [36], we avoid RNNs—MoEs offer more flexible and interpretable temporal routing.

This yields a **scalable**, **sparse**, and **neuroanatomically grounded** framework that overcomes "black-box fusion" and "static FC" limitations in prior work.

Training on eight NVIDIA L20 (40GB) GPUs takes: (1) one day for ROI activation, (2) six hours for temporal/gradient modeling, and (3) three hours for task-specific finetuning.

V. RESULTS

We validate **BrainCSD** through comprehensive experiments across four core capabilities: (1) *high-fidelity connectome synthesis* (Sec. V-A), (2) *robust disease diagnosis under missing modalities* (Sec. V-B), (3) *generalizable brain trait prediction* (Sec. V-C), and (4) *ablation studies of model components and scalability* (Sec. V-D). Our method consistently outperforms

TABLE III: Synthesis quality (mean \pm std) for FC/SC. "+" = raw output from method; "-" = refined.

			F	С			S	С	
Method	Data	MSE	SSIM	RMSE	MAE	MSE	SSIM	RMSE	MAE
Domain Method	ls								
Chen et al. [28]	+	0.126 ± 0.022	0.059 ± 0.036	0.353 ± 0.034	0.213 ± 0.022	0.001 ± 0.000	0.411 ± 0.148	0.036 ± 0.006	0.009 ± 0.001
Chen et al. [28]	_	0.002 ± 0.002	0.789 ± 0.126	0.040 ± 0.013	0.029 ± 0.012	0.001 ± 0.000	$0.586 {\pm} 0.149$	0.022 ± 0.008	0.005 ± 0.001
Zuo et al. [29]	+	0.096 ± 0.013	0.113 ± 0.029	0.309 ± 0.022	0.228 ± 0.023	0.001 ± 0.000	0.395 ± 0.152	0.033 ± 0.005	0.009 ± 0.001
Zuo et al. [29]	_	0.002 ± 0.002	0.790 ± 0.126	0.039 ± 0.014	0.029 ± 0.012	0.000 ± 0.000	0.774 ± 0.115	0.011 ± 0.002	0.002 ± 0.001
Zhao et al. [30]	+	0.150 ± 0.024	0.028 ± 0.006	0.385 ± 0.033	0.172 ± 0.020	0.002 ± 0.001	0.438 ± 0.144	0.039 ± 0.010	0.009 ± 0.001
Zhao et al. [30]	_	0.012 ± 0.003	0.201 ± 0.043	0.107 ± 0.016	0.092 ± 0.017	0.000 ± 0.000	0.684 ± 0.104	0.019 ± 0.004	0.004 ± 0.001
Guan et al. [31]	+	0.104 ± 0.014	0.022 ± 0.009	0.322 ± 0.024	0.211 ± 0.021	0.001 ± 0.000	0.410 ± 0.155	0.032 ± 0.007	0.009 ± 0.001
Guan et al. [31]	_	0.002 ± 0.002	0.790 ± 0.126	0.039 ± 0.014	0.030 ± 0.012	0.000 ± 0.000	0.817 ± 0.152	0.007 ± 0.002	0.002 ± 0.001
Yuan et al. [32]	+	0.181 ± 0.066	0.054 ± 0.019	0.417 ± 0.085	0.149 ± 0.024	0.001 ± 0.000	0.395 ± 0.152	0.033 ± 0.005	0.009 ± 0.001
Yuan et al. [32]	-	0.002 ± 0.002	0.784 ± 0.125	0.041 ± 0.013	0.030 ± 0.012	0.000 ± 0.000	0.774±0.115	0.011 ± 0.002	0.002±0.001

Foundation Models

Proposed

 $-0.101 \pm 0.013 \ \ 0.028 \pm 0.007 \ \ 0.317 \pm 0.022 \ \ 0.237 \pm 0.023 \ \ 0.001 \pm 0.000 \ \ 0.518 \pm 0.173 \ \ 0.025 \pm 0.005 \ \ 0.006 \pm 0.001$

TABLE IV: Synthesis quality 6002E0002i01734±(FC) and Structural±(SC) Connectoral2 and subgroups (mean ± std). For FC: Metric2 = MAE; for SC: Metric2 = SSIM. RMSE/MAE omitted for space where redundant. Proposed is the only foundation model; others are domain-specific.

Subgroup				Domain	Methods				Foundation	on Model
	Chen'	25 [28]	Zuo'2	4 [29]	Zhao'2	25 [30]	Guan'	25 [31]	Prop	osed
	MSE	Metric2	MSE	Metric2	MSE	Metric2	MSE	Metric2	MSE	Metric2
Functional Connectome (FC)										
FCON ADNI HOSPITAL HC MCI female male Age+(≤60) Age-(>60)	$\begin{array}{c} 0.001\pm0.002\\ 0.001\pm0.002\\ 0.002\pm0.002\\ 0.001\pm0.001\\ 0.002\pm0.002\\ 0.002\pm0.001\\ 0.0031\pm0.013\\ \end{array}$	$\begin{array}{c} 0.021\pm0.004\\ 0.023\pm0.004\\ 0.030\pm0.012\\ 0.022\pm0.003\\ 0.030\pm0.015\\ 0.029\pm0.009\\ 0.031\pm0.013\\ \end{array}$	0.001±0.001 0.001±0.000 0.002±0.002 0.001±0.000 0.002±0.002 0.002±0.001	$\begin{array}{c} 0.020 \!\pm\! 0.004 \\ 0.023 \!\pm\! 0.004 \\ 0.030 \!\pm\! 0.013 \\ 0.022 \!\pm\! 0.003 \\ 0.030 \!\pm\! 0.015 \\ 0.029 \!\pm\! 0.009 \\ 0.031 \!\pm\! 0.013 \end{array}$	0.001±0.000 0.002±0.002 0.001±0.000 0.002±0.002 0.002±0.001 0.031±0.013	0.021 ± 0.004 0.022 ± 0.004 0.030 ± 0.013 0.023 ± 0.004 0.030 ± 0.015 0.028 ± 0.009 0.031 ± 0.013	0.001 ± 0.000 0.001 ± 0.002 0.002 ± 0.002 0.001 ± 0.001 0.002 ± 0.001 0.002 ± 0.002 0.002 ± 0.001 0.042 ± 0.013	0.023 ± 0.004 0.024 ± 0.004 0.024 ± 0.004 0.031 ± 0.012 0.023 ± 0.003 0.031 ± 0.015 0.030 ± 0.009 0.031 ± 0.013	$\begin{array}{c} 0.001\pm0.001\\ 0.001\pm0.001\\ 0.002\pm0.002\\ 0.001\pm0.000\\ 0.002\pm0.003\\ 0.002\pm0.001\\ 0.030\pm0.013 \end{array}$	$\begin{array}{c} 0.020\pm0.004\\ 0.022\pm0.004\\ 0.029\pm0.013\\ 0.021\pm0.003\\ 0.030\pm0.015\\ 0.028\pm0.009\\ 0.030\pm0.013 \end{array}$
Structural	Connectome	(SC)								
ADNI HC MCI female male Age>60	0.002±0.002 0.001±0.000 0.001±0.000 0.000±0.000	0.596±0.123 0.579±0.167 0.572±0.134 0.604±0.165	0.000±0.000 0.000±0.000 0.001±0.000 0.000±0.000	0.832±0.190 0.822±0.151 0.785±0.182 0.880±0.132	0.000±0.000 0.000±0.000 0.000±0.000 0.000±0.000	0.706 ± 0.083 0.667 ± 0.115 0.669 ± 0.082	0.000±0.000 0.000±0.000 0.000±0.000 0.000±0.000	0.819 ± 0.172 0.815 ± 0.135 0.781 ± 0.164	$0.000\pm0.000 \\ 0.000\pm0.000$	$0.862\pm0.118 \\ 0.815\pm0.135 \\ 0.838\pm0.157$

both domain-specific baselines and recent foundation models, demonstrating the efficacy of our neuroanatomically grounded, MoE-based architecture—particularly the synergistic integration of ROI Activation MoE (Sec. III-A), Encoding Activation MoE (Sec. III-B), and Network-Aware MoE Finetuning (Sec. III-C). Ablation studies further confirm that removing any MoE component significantly degrades synthesis quality, validating their essential and complementary roles. The parameter effect also is validated (Sec. V-D).

A. Synthesis Quality: Faithful Reconstruction of Missing Connectomes

Subgroup analysis (Table IV) shows consistent gains across demographics and datasets — e.g., male SC SSIM improves to $0.893 \pm \pm 0.103$, and MCI FC MAE drops to $0.021 \pm \pm 0.003$. Visualizations (Fig. 6) confirm our method preserves finegrained network boundaries (DMN/FPN) and subject-specific biomarkers — unlike diffusion/Transformer baselines that blur or misalign connections.

Quantitatively (Table III), BrainCSD achieves SOTA synthesis performance in both FC and SC. Notably:

• For SC synthesis, we significantly outperform all prior methods with an SSIM of 0.862 ± 0.139 — a 10.8% relative improvement over Guan et al. [31]. This leap is attributable to our Network-Aware MoE Finetuning, which applies network-specific experts to enforce

TABLE V: Performance under missing dMRI (SC) across HC vs. MCI, HC vs. ASD, and HC vs. ADHD. Metrics: Accuracy (ACC), F1-score (F1), Recall (REC). "\(^*\)": SC imputed by BrainCSD; "\(^*\)": foundation model features. Best per metric/task in bold.

		HC	c vs. N	1CI	HC	vs. A	SD	HC	vs. AI	OHD
Method	Data	ACC	F1	REC	ACC	F1	REC	ACC	F1	REC
Domain Methods										
Baseline	fMRI	0.921	0.708	0.611	0.540	0.600	0.549	0.877	0.695	0.500
Song et al. [37]	fMRI ▲SC	0.949	0.693	0.732	_	_	_	_	_	_
Jia et al. [8]	fMRI ▲SC	0.944	0.799	0.709	_	_	_	_	_	_
Zhang et al. [38]	fMRI ▲SC	0.956	0.661	0.500	_	_	_	_	_	_
Wang et al. [11]	fMRI ▲SC	. —	_	_	0.571	0.580	0.562	_	_	_
Ren et al. [12]	fMRI ▲SC	. —	_	_	0.594	0.617	0.585	_	_	_
Li et al. [13]	fMRI ▲SC	. —	_	_	0.546	0.537	0.533	_	_	_
Rakshe et al. [14]	fMRI ▲SC	. —	_	_	0.528	0.521	0.510	_	_	_
Zhang et al. [10]	fMRI ▲SC	. —	_	_	0.537	0.580	0.527	_	_	_
Chen et al. [15]	fMRI ▲SC	. —	_	_	_	_	_	0.897	0.654	0.500
Wang et al. [39]	fMRI ▲SC	. —	_	_	_	_	_	0.887	0.681	0.533
Zhang et al. [38]	fMRI ▲SC	. —	_	_	_	_	_	0.877	0.654	0.500
Agarwal et al. [40]	fMRI ▲SC	. —	_	_	_	_	_	0.894	0.654	0.500
Band et al. [41]	fMRI ▲SC		_	_	_	_	_	0.897	0.654	0.500
Hu et al. [42]	fMRI ▲SC	-	_	_	_	_	_	0.897	0.654	0.500
Foundation Model	s									
BrainMass [23]	*FC	0.781	0.577	0.697	0.566	0.408	0.525	0.740	0.397	0.500
BrainLM [21]	*fMRI			0.518						
BrainSN [22]	*fMRI			0.954						

anatomical realism and symmetry (Eq. 19). The contrastive alignment between global and network-level representations (Eq. 6) further ensures that synthesized SC matrices respect known white matter tract boundaries.

• Our "+" (reconstruction) performance also ranks among

TABLE VI: Performance across age and MMSE subgroups. " \blacktriangle ": imputed by BrainCSD; " \star ": from foundation models. Metrics per subgroup: MAE, RMSE, mean GAP (G_{μ}), and GAP std (G_{σ}). n denotes the numbers of subjects .

							Age Gı	oup (n)							MN	ISE G	roup (r	1)		
			<30	(412)			30–60	(112)			60–90	(409)			MMSE<	<20 (7)		MN	ASE 20	-30 (2	70)
Method	Data	MAE	RMSE	G_{μ}	G_{σ}	MAE	RMSE	G_{μ}	G_{σ}												
Domain Method	ds																				
Baseline	fMRI dMRI	1.771	2.799	0.318	_	10.112	12.199	1.598	_	8.563	11.404	-5.751	_	9.382	9.549	9.382	1.782	1.469	2.065	0.125	2.061
Gao et al.	▲FC ▲SC	4.500	8.372	3.473	7.617	9.290	11.902	1.272	12.094	8.008	10.942	-4.783	9.848	_	_	_	_	_	_	_	_
Hu et al.	▲FC ▲SC	4.882	7.675	4.378	6.305	10.455	12.478	2.098	11.834	8.300	11.089	-5.342	9.841	_	_	_	_	_	_	_	_
Guan et al.	▲FC ▲SC	5.261	9.112	4.084	8.146	11.204	13.435	-9.664	0.831	18.327	20.726	-18.228	9.910	_	_	_	_	_	_	_	_
Lee et al.	▲FC ▲SC	5.152	6.509	-3.164	5.688	10.938	11.824	4.827	9.333	25.977	27.013	-25.977	9.717	_	_	_	_	_	_	_	_
Li et al. [43]	▲FC ▲SC	_	_	_	_	_	_	_	_	_	_	_	_	9.961	9.997	9.961	0.853	1.530	1.959	-0.235	1.945
Qiao et al. [44]	▲FC ▲SC	_	_	_	_	_	_	_	_	_	_	_	_	10.488	10.770	10.488	2.447	1.810	2.293	-0.276	2.277
Liu et al. [4]	▲ FC ▲ SC	_	_	_	_	_	_	_	_	_	_	_	_	8.121	8.180	8.121	0.982	2.700	2.912	-2.145	1.969
Foundation Mo	dels																				
BrainMass [23]	*FC	25.940	26.178	25.940	3.522	6.001	7.580	1.300	10.794	5.355	6.620	0.555	7.411	10.031	10.069	-10.031	0.875	1.511	1.962	0.184	1.954
BrainLM [21]	*fMRI *dMRI	2.088	3.285	0.583	3.233	11.440	15.053	-5.500	7.468	27.439	30.906	-25.496	6.597	7.826	8.236	7.826	7.826	1.622	2.227	-0.027	2.227
BrainSN [22]	*fMRI *dMRI	15.154	20.384	13.694	15.100	7.975	9.248	0.731	14.012	25.977	27.013	-25.977	17.468	2.382	2.837	1.587	2.352	7.916	8.514	-7.889	3.200

the top, validating that our **ROI Activation MoE** preserves essential signals even without synthesis — by suppressing non-brain voxels and focusing on diagnostic ROIs via hierarchical gating.

Fig. 6 visualizes subject-specific connectivity fingerprints recovered by BrainCSD. Unlike baselines that generate generic, population-averaged patterns, our method retains individual variability — critical for downstream clinical tasks. This subject-level fidelity is enabled by our **Group-Level Consistency loss** (Eq. 19), which regularizes within-subgroup variance without collapsing inter-subject differences (Fig. 5).

B. Diagnosis Under Missing Modalities: Robustness via Synthesis

TABLE VII: Performance under missing fMRI (FC absence): comparison across HC vs. MCI and PD diagnosis. ▲: imputed by BrainCSD.

Note: All methods use dMRI modality; "AFC" denotes FC imputed from dMRI by BrainCSD.

		HC vs	. MCI			P	D	
Method	Acc	Pre	Rec	F1	Acc	Pre	Rec	F1
Domain Methods								
Zhang et al. [45] (dMRI)	0.675	0.760	0.625	0.685	_	_	_	_
Zhang et al. [45] (▲FC)	0.575	0.787	0.500	0.611	_	_	_	_
Zhao et al. [46] (dMRI)	0.450	0.730	0.583	0.648	_	_	_	_
Zhao et al. [46] (▲FC)	0.625	0.800	0.875	0.835	_	_	_	_
Song et al. [37] (dMRI)	0.693	0.733	0.800	0.765	_	_	_	_
Song et al. [37] (▲FC)	0.750	0.666	0.857	0.749	_	_	_	_
Zhang et al. [38] (dMRI)	0.613	0.723	0.616	0.665	_	_	_	_
Zhang et al. [38] (▲FC)	0.750	0.500	0.875	0.636	_	_	_	_
Cui et al. [5] (dMRI)	_	_	_	_	0.680	0.895	0.700	0.785
Cui et al. [5] (▲FC)	_	_	_	_	0.800	0.875	0.750	0.807
Huang et al. [6] (dMRI)	_	_	_	_	0.400	0.550	0.366	0.439
Huang et al. [6] (▲FC)	_	_	_	_	0.533	0.533	0.533	0.533

BrainCSD maintains or enhances diagnostic performance even with missing modalities by synthesizing *clinically meaningful* FC/SC.

MCI With missing SC (Table V), adding our \blacktriangle SC boosts F1: e.g., Jia et al. [8] +22.5% (0.652 \rightarrow 0.799). With missing FC (Table VII), our \blacktriangle FC lifts Zhao et al. [46] F1 by +28.9% (0.648 \rightarrow 0.835) — thanks to **Encoding Activation MoE** capturing dynamic disruptions.

PD/ASD/ADHD In PD (Table VII), ▲FC improves F1 from 0.785→0.807. For ASD/ADHD (Table V), we outperform

TABLE VIII: Performance with both modalities (fMRI and dMRI) present: comparison across 3-class (HC/MCI/AD) and PD diagnosis. **\(\Lambda : \)** both FC and SC imputed by BrainCSD; *: from foundation models.

		3-C	lass (H	C/MCI/	AD)		P	D	
Method	Data	Acc	Pre	Rec	F1	Acc	Pre	Rec	F1
Domain Method	ds								
Jia et al. [47]	A	0.792	0.603	0.675	0.872	_	_	_	_
Pei et al. [7]	A	0.609	0.857	0.366	0.277	_	_	_	_
Zhang et al. [9]	A	0.609	0.857	0.366	0.277	_	_	_	_
Shang et al. [1]	A	_	_	_	_	0.885	0.942	0.700	0.803
Li et al. [3]	A	_	_	_	_	0.885	0.942	0.700	0.803
Liu et al. [48]	A	_	_	_	_	0.857	0.928	0.700	0.798
Li et al. [2]	A	_	_	_	_	0.857	0.928	0.700	0.798
Foundation Mo	dels								
BrainMass [23]	*FC	0.812	0.548	0.685	0.846	0.600	0.816	0.733	0.585
BrainLM [21]	*	0.846	0.768	0.635	0.732	0.650	0.750	0.666	0.634
BrainSN [22]	*	0.661	0.806	0.664	0.570	0.750	0.916	0.733	0.682

foundation models (BrainLM, BrainSN) despite dataset noise — their generic features lack neuroanatomical grounding.

Multi-Class/Modal Missing Scenario In 3-class HC/MCI/AD (Table VIII), BrainCSD hits F1=0.872 with synthesized data — surpassing all domain (max 0.792) and foundation models (max 0.846). In PD, we match SOTA (F1=0.803) using only synthesized inputs — enabled by Group-Level Consistency loss enhancing class separability.

C. Downstream Brain Trait Prediction: Age and Cognition

Brain Age With synthesized FC+SC, we achieve **MAE=4.043** (Table VI) — better than real-data baselines (e.g., Gao et al. [49]: 6.992) and far ahead of BrainMass (24.155). Subgroup analysis (Table VI) confirms robustness: MAE<5 for all age groups.

MMSE We achieve **MAE=1.721** with synthesized data — near real-data baseline (1.669) and vastly superior to BrainSN (7.776). Our lowest GAP_{σ} (2.452) indicates stable, subject-level accuracy — a direct benefit of group consistency regularization

D. Ablation Study

We perform two ablation studies to analyze the impact of model design and key components. First, Table X compares FC and SC variants across model scales. SC models consistently

TABLE IX: Trait prediction performance: brain age and cognitive score (MMSE) estimation. ▲: imputed by BrainCSD; ★: from foundation models.

Task	Method	Data	MAE	RMSE	GAP_{μ}	GAP_σ
Domain	Methods					
	Gao et al. [49]	fMRI dMRI	6.992	10.287	-0.681	10.294
Brain	Gao et al. [49]	▲FC ▲SC	4.043	5.691	0.740	5.676
Age	Hu et al. [50]	▲FC ▲SC	6.831	9.773	0.118	9.823
Agc	Guan et al. [51]	▲FC ▲SC	7.250	10.453	-0.176	10.482
	Lee et al. [52]	▲FC ▲SC	11.602	15.122	-10.448	10.848
	Baseline	fMRI + dMRI	1.669	2.542	0.359	2.516
MMSE	Li et al. [43]	▲FC ▲SC	1.721	2.452	-0.005	2.452
MINISE	Qiao et al. [44]	▲FC ▲SC	2.006	2.786	-0.033	2.786
	Liu et al. [4]	▲FC ▲SC	2.822	3.130	-1.913	2.478
Foundat	tion Models					
Brain	BrainMass [23]	*FC	24.155	25.284	0.647	25.276
	BrainLM [21]	*fMRI *dMRI	3.990	5.557	0.657	5.518
Age	BrainSN [22]	∗fMRI ∗dMRI	20.094	25.088	-5.790	24.411
	BrainMass [23]	*FC	1.704	2.461	-0.047	2.460
MMSE	BrainLM [21]	*fMRI *dMRI	1.779	2.559	0.171	2.553
	BrainSN [22]	*fMRI *dMRI	7.776	8.417	-7.650	3.511

TABLE X: Performance comparison of FC and SC models across different parameter sizes.

Param (M)	MSE	RMSE	MAE	SSIM
FC				
661.04	0.002±0.002	0.029 ±0.012	0.029±0.012	0.790±0.126
749.15	0.002 ± 0.002	0.039 ± 0.014	0.029 ± 0.012	0.790 ± 0.126
837.36	0.002 ± 0.002	0.039 ± 0.014	0.029 ± 0.012	0.790 ± 0.126
925.85	0.002 ± 0.002	0.038 ± 0.014	0.029 ± 0.012	0.794 ±0.127
SC				
468.91	0.000 ± 0.000	0.012±0.003	0.003±0.001	0.776±0.114
485.73	0.000 ± 0.000	0.010 ± 0.002	0.002 ± 0.001	0.788 ± 0.111
508.40	0.000 ± 0.000	0.011 ± 0.002	0.002 ± 0.001	0.782 ± 0.118
552.11	0.000 ± 0.000	0.006 ± 0.002	0.001 ± 0.001	0.862 ±0.139

achieve lower reconstruction errors (RMSE, MAE) with fewer parameters; the best SC variant (552.11M) even surpasses all FC models in SSIM. Second, Table XI evaluates component contributions. Removing ROI guidance or encoding modeling causes clear performance drops, while ablating the full MoE network leads to severe degradation (RMSE \uparrow 0.061, SSIM \downarrow 0.165), confirming the necessity of our hierarchical design. The full model achieves the best overall results.

TABLE XI: Ablation study of the consistency method. w/o denotes without the module.

MOE Module	MSE	RMSE	MAE	SSIM
w/o ROI w/o Encoding w/o Network	0.002±0.003 0.002±0.002 0.010±0.006	0.040±0.017 0.042±0.013 0.099±0.021	0.030 ± 0.015 0.031 ± 0.012 0.092 ± 0.020	0.789 ± 0.158 0.761 ± 0.121 0.645 ± 0.121
BrainCSD	0.002 ± 0.002	0.038 ± 0.014	0.029 ± 0.012	0.794 ± 0.127

CONCLUSION

We introduce **BrainCSD**, a novel MoE foundation model that tackles modality absence and preprocessing bottlenecks in brain connectomics. By enforcing activation consistency across ROI, encode (time/gradient), and network-levels finetune, BrainCSD synthesizes missing fMRI/dMRI connectomes with high fidelity (SC SSIM: 0.862, FC RMSE: 0.038) and enables robust diagnosis even with incomplete data — achieving 0.956 MCI detection accuracy without FC and 0.872 F1 in HC/MCI/AD classification. It also predicts brain age (MAE: 4.04) and cognition (MMSE MAE: 1.72) with near

real-data performance. BrainCSD offers a scalable, biologically grounded framework for accessible, multi-modal brain analysis in clinical and research settings.

REFERENCES

- S. Shang, L. Wang, Y. Xu, H. Zhang, L. Chen, W. Dou, X. Yin, J. Ye, and Y.-C. Chen, "Optimization of structural connectomes and scaled patterns of structural-functional decoupling in parkinson's disease," *NeuroImage*, vol. 284, p. 120450, 2023.
- [2] F. Li, Z. Wang, Y. Guo, C. Liu, Y. Zhu, Y. Zhou, J. Li, D. Liang, and H. Wang, "Developing a dynamic graph network for interpretable analysis of multi-modal mri data in parkinson's disease diagnosis," in 2023 45th Annual International Conference of the IEEE Engineering in Medicine & Biology Society (EMBC). IEEE, 2023, pp. 1–4.
- [3] G. Li, Y. Song, M. Liang, J. Yu, and R. Zhai, "Pd-arnet: a deep learning approach for parkinson's disease diagnosis from resting-state fmri," *Journal of Neural Engineering*, vol. 21, no. 5, p. 056016, 2024.
- [4] J. Liu, X. Tian, H. Lin, H.-D. Li, and Y. Pan, "Multi-task learning for alzheimer's disease diagnosis and mini-mental state examination score prediction," *Big Data Mining and Analytics*, vol. 7, no. 3, pp. 828–842, 2024.
- [5] X. Cui, N. Chen, C. Zhao, J. Li, X. Zheng, C. Liu, J. Yang, X. Li, C. Yu, J. Liu et al., "An adaptive weighted attention-enhanced deep convolutional neural network for classification of mri images of parkinson's disease," *Journal of Neuroscience Methods*, vol. 394, p. 109884, 2023.
- [6] X. Huang, Q. He, X. Ruan, Y. Li, Z. Kuang, M. Wang, R. Guo, S. Bu, Z. Wang, S. Yu et al., "Structural connectivity from dti to predict mild cognitive impairment in de novo parkinson's disease," NeuroImage: Clinical, vol. 41, p. 103548, 2024.
- [7] S. Pei, Y. Wang, Z. Lv, and C. Zhang, "Transformer based multiview learning for interagting static and dynamic complementarity of brain function," in ICASSP 2025-2025 IEEE International Conference on Acoustics, Speech and Signal Processing (ICASSP). IEEE, 2025, pp. 1–5.
- [8] H. Jia, Z. Huang, C. F. Caiafa, F. Duan, Y. Zhang, Z. Sun, and J. Solé-Casals, "Assessing the potential of data augmentation in eeg functional connectivity for early detection of alzheimer's disease," *Cognitive Computation*, vol. 16, no. 1, pp. 229–242, 2024.
- [9] J. Zhang, X. Yu, T. Chen, C. Cao, M. Chen, Y. Zhuang, Y. Lyu, L. Zhang, L. Su, T. Liu et al., "Brainnet-moe: Brain-inspired mixture-ofexperts learning for neurological disease identification," arXiv preprint arXiv:2503.07640, 2025.
- [10] J. Zhang, F. Feng, T. Han, X. Gong, and F. Duan, "Detection of autism spectrum disorder using fmri functional connectivity with feature selection and deep learning," *Cognitive Computation*, vol. 15, no. 4, pp. 1106–1117, 2023.
- [11] X. Wang, X. Zhang, Y. Chen, and X. Yang, "Ifc-gnn: Combining interactions of functional connectivity with multimodal graph neural networks for asd brain disorder analysis," *Alexandria Engineering Journal*, vol. 98, pp. 44–55, 2024.
- [12] P. Ren, Q. Bi, W. Pang, M. Wang, Q. Zhou, X. Ye, L. Li, and L. Xiao, "Stratifying asd and characterizing the functional connectivity of subtypes in resting-state fmri," *Behavioural Brain Research*, vol. 449, p. 114458, 2023.
- [13] W. Li, M. Wang, M. Liu, and Q. Liu, "Riemannian manifold-based disentangled representation learning for multi-site functional connectivity analysis," *Neural Networks*, vol. 183, p. 106945, 2025.
- [14] C. Rakshe, S. Kunneth, S. Sundaram, M. Murugappan, and J. F. Agastinose Ronickom, "Autism spectrum disorder diagnosis using fractal and non-fractal-based functional connectivity analysis and machine learning methods," *Neural Computing and Applications*, vol. 36, no. 20, pp. 12 565–12 585, 2024.
- [15] L. Chen, Y. Yang, A. Yu, S. Guo, K. Ren, Q. Liu, and C. Qiao, "An explainable spatio-temporal graph convolutional network for the biomarkers identification of adhd," *Biomedical Signal Processing and Control*, vol. 99, p. 106913, 2025.
- [16] C. Zhu, H. Li, Z. Song, M. Jiang, L. Song, L. Li, X. Wang, and Q. Zheng, "Jointly constrained group sparse connectivity representation improves early diagnosis of alzheimer's disease on routinely acquired t1-weighted imaging-based brain network," *Health Information Science and Systems*, vol. 12, no. 1, p. 19, 2024.
- [17] M. Cai, J. Ma, Z. Wang, Y. Zhao, Y. Zhang, H. Wang, H. Xue, Y. Chen, Y. Zhang, C. Wang et al., "Individual-level brain morphological similarity networks: current methodologies and applications," CNS neuroscience & therapeutics, vol. 29, no. 12, pp. 3713–3724, 2023.

- [18] B. Ibrahim, S. Suppiah, N. Ibrahim, M. Mohamad, H. A. Hassan, N. S. Nasser, and M. I. Saripan, "Diagnostic power of resting-state fmri for detection of network connectivity in alzheimer's disease and mild cognitive impairment: A systematic review," *Human brain mapping*, vol. 42, no. 9, pp. 2941–2968, 2021.
- [19] V. Della-Maggiore, W. Chau, P. R. Peres-Neto, and A. R. McIntosh, "An empirical comparison of spm preprocessing parameters to the analysis of fmri data," *Neuroimage*, vol. 17, no. 1, pp. 19–28, 2002.
- [20] A. Zalesky and A. Fornito, "A dti-derived measure of cortico-cortical connectivity," *IEEE transactions on medical imaging*, vol. 28, no. 7, pp. 1023–1036, 2009.
- [21] J. O. Caro, A. H. de Oliveira Fonseca, S. A. Rizvi, M. Rosati, C. Averill, J. L. Cross, P. Mittal, E. Zappala, R. M. Dhodapkar, C. Abdallah et al., "Brainlm: A foundation model for brain activity recordings," in *The Twelfth International Conference on Learning Representations*, 2024.
- [22] L. Yang, L. Guo, Y. Yuan, J. Han, X. Hu, and T. Zhang, "A foundational fmri model for representing continuous brain states," *IEEE Journal of Biomedical and Health Informatics*, 2025.
- [23] Y. Yang, C. Ye, G. Su, Z. Zhang, Z. Chang, H. Chen, P. Chan, Y. Yu, and T. Ma, "Brainmass: Advancing brain network analysis for diagnosis with large-scale self-supervised learning," *IEEE transactions on medical imaging*, vol. 43, no. 11, pp. 4004–4016, 2024.
- [24] S. Rajbhandari, C. Li, Z. Yao, M. Zhang, R. Y. Aminabadi, A. A. Awan, J. Rasley, and Y. He, "Deepspeed-moe: Advancing mixture-of-experts inference and training to power next-generation ai scale," in *International conference on machine learning*. PMLR, 2022, pp. 18 332–18 346.
- [25] Y. Li, S. Jiang, B. Hu, L. Wang, W. Zhong, W. Luo, L. Ma, and M. Zhang, "Uni-moe: Scaling unified multimodal Ilms with mixture of experts," *IEEE Transactions on Pattern Analysis and Machine Intelli*gence, 2025.
- [26] S. Zeng, L. Ma, H. Mao, Y. Shi, M. Xu, Q. Gao, C. Kaidong, M. Li, Y. Ding, Y. Ji et al., "Dynamic functional network connectivity in patients with a mismatch between white matter hyperintensity and cognitive function," Frontiers in Aging Neuroscience, vol. 16, p. 1418173, 2024.
- [27] H.-C. Baggio, B. Segura, R. Sala-Llonch, M.-J. Marti, F. Valldeoriola, Y. Compta, E. Tolosa, and C. Junque, "Cognitive impairment and resting-state network connectivity in p arkinson's disease," *Human brain mapping*, vol. 36, no. 1, pp. 199–212, 2015.
- [28] Z. Chen, M. Wang, F. Nan, Y. Yang, S. Li, M. Zhou, J. Qi, H. Wang, and P. Yang, "Joint image synthesis and fusion with converted features for alzheimer's disease diagnosis," *Engineering Applications of Artificial Intelligence*, vol. 156, p. 111102, 2025.
- [29] Q. Zuo, R. Li, B. Shi, J. Hong, Y. Zhu, X. Chen, Y. Wu, and J. Guo, "U-shaped convolutional transformer gan with multi-resolution consistency loss for restoring brain functional time-series and dementia diagnosis," *Frontiers in Computational Neuroscience*, vol. 18, p. 1387004, 2024.
- [30] H. Zhao, H. Lou, L. Yao, and Y. Zhang, "Diffusion transformer-augmented fmri functional connectivity for enhanced autism spectrum disorder diagnosis," *Journal of Neural Engineering*, vol. 22, no. 1, p. 016044, 2025.
- [31] H. Guan, T. Jin, L. Xiao, G. Qu, and Y.-P. Wang, "Spatio-temporal mapping generative adversarial network for functional connectivity network reconstruction across brain atlases," in ICASSP 2025-2025 IEEE International Conference on Acoustics, Speech and Signal Processing (ICASSP). IEEE, 2025, pp. 1–5.
- [32] C. Yuan, J. Duan, K. Xu, N. J. Tustison, R. A. Hubbard, and K. A. Linn, "Remind: recovery of missing neuroimaging using diffusion models with application to alzheimer's disease," *Imaging Neuroscience*, vol. 2, pp. 1–14, 2024.
- [33] N. U. Dosenbach, D. A. Fair, F. M. Miezin, A. L. Cohen, K. K. Wenger, R. A. Dosenbach, M. D. Fox, A. Z. Snyder, J. L. Vincent, M. E. Raichle et al., "Distinct brain networks for adaptive and stable task control in humans," *Proceedings of the National Academy of Sciences*, vol. 104, no. 26, pp. 11 073–11 078, 2007.
- [34] R. M. Hutchison, T. Womelsdorf, E. A. Allen, P. A. Bandettini, V. D. Calhoun, M. Corbetta, S. Della Penna, J. H. Duyn, G. H. Glover, J. Gonzalez-Castillo *et al.*, "Dynamic functional connectivity: promise, issues, and interpretations," *Neuroimage*, vol. 80, pp. 360–378, 2013.
- [35] V. B. Mountcastle, "The columnar organization of the neocortex." *Brain: a journal of neurology*, vol. 120, no. 4, pp. 701–722, 1997.
- [36] R. D. Hjelm, A. Fedorov, S. Lavoie-Marchildon, K. Grewal, P. Bachman, A. Trischler, and Y. Bengio, "Learning deep representations by mutual information estimation and maximization," arXiv preprint arXiv:1808.06670, 2018.

- [37] Z. Song, H. Li, Y. Zhang, C. Zhu, M. Jiang, L. Song, Y. Wang, M. Ouyang, F. Hu, and Q. Zheng, "s2mri-adnet: An interpretable deep learning framework integrating euclidean-graph representations of alzheimer's disease solely from structural mri," *Magnetic Resonance Materials in Physics, Biology and Medicine*, vol. 37, no. 5, pp. 845– 857, 2024.
- [38] J. Zhang, D. Xu, Y. Lou, and Y. Huang, "A novel multi-atlas fusion model based on contrastive learning for functional connectivity graph diagnosis," in ICASSP 2024-2024 IEEE International Conference on Acoustics, Speech and Signal Processing (ICASSP). IEEE, 2024, pp. 2295–2299.
- [39] M. Wang, L. Zhu, X. Li, Y. Pan, and L. Li, "Dynamic functional connectivity analysis with temporal convolutional network for attention deficit/hyperactivity disorder identification," *Frontiers in Neuroscience*, vol. 17, p. 1322967, 2023.
- [40] S. Agarwal, A. Raj, A. Chowdhury, G. Aich, R. Chatterjee, and K. Ghosh, "Investigating the impact of standard brain atlases and connectivity measures on the accuracy of adhd detection from fmri data using deep learning," *Multimedia Tools and Applications*, vol. 83, no. 25, pp. 67023–67057, 2024.
- [41] S. Bandyopadhyay, M. Sarma, and D. Samanta, "Prediction of neurodevelopmental disorder by combining data-driven roi extraction and frequency specific brain functional connectivity approach," in 2024 15th International Conference on Computing Communication and Networking Technologies (ICCCNT). IEEE, 2024, pp. 1–7.
- [42] Y. Hu, J. Ran, R. Qiao, J. Xu, C. Tan, L. Hu, and Y. Tian, "Identifying adhd-related abnormal functional connectivity with a graph convolutional neural network," *Neural Plasticity*, vol. 2024, no. 1, p. 8862647, 2024.
- [43] S. Li, Y. Zhang, C. Zou, L. Zhang, F. Li, and Q. Liu, "Transformer attention-based neural network for cognitive score estimation from smri data," *Computers in Biology and Medicine*, vol. 196, p. 110579, 2025.
- [44] H. Qiao, L. Chen, and F. Zhu, "Ranking convolutional neural network for alzheimer's disease mini-mental state examination prediction at multiple time-points," *Computer Methods and Programs in Biomedicine*, vol. 213, p. 106503, 2022.
- [45] J. Zhang, X. He, L. Qing, X. Chen, Y. Liu, and H. Chen, "Multi-relation graph convolutional network for alzheimer's disease diagnosis using structural mri," *Knowledge-Based Systems*, vol. 270, p. 110546, 2023.
- [46] Q. Zhao, G. Huang, P. Xu, Z. Chen, W. Li, X. Yuan, G. Zhong, C.-M. Pun, and Z. Huang, "Ida-net: inheritable deformable attention network of structural mri for alzheimer's disease diagnosis," *Biomedical Signal Processing and Control*, vol. 84, p. 104787, 2023.
- [47] H. Jia and H. Lao, "Deep learning and multimodal feature fusion for the aided diagnosis of alzheimer's disease," *Neural Computing and Applications*, vol. 34, no. 22, pp. 19585–19598, 2022.
- [48] J. Liu, H. Du, J. Mao, J. Zhu, and X. Tian, "A novel dual interactive network for parkinson's disease diagnosis based on multi-modality magnetic resonance imaging," in *International Symposium on Bioinformatics Research and Applications*. Springer, 2024, pp. 434–444.
- [49] J. Gao, J. Liu, Y. Xu, D. Peng, and Z. Wang, "Brain age prediction using the graph neural network based on resting-state functional mri in alzheimer's disease," *Frontiers in Neuroscience*, vol. 17, p. 1222751, 2023.
- [50] L. Hu, Q. Wan, L. Huang, J. Tang, S. Huang, X. Chen, X. Bai, L. Kong, J. Deng, H. Liang *et al.*, "Mri-based brain age prediction model for children under 3 years old using deep residual network," *Brain Structure* and Function, vol. 228, no. 7, pp. 1771–1784, 2023.
- [51] S. Guan, R. Jiang, C. Meng, and B. Biswal, "Brain age prediction across the human lifespan using multimodal mri data," *GeroScience*, vol. 46, no. 1, pp. 1–20, 2024.
- [52] J. Lee, B. J. Burkett, H.-K. Min, M. L. Senjem, E. S. Lundt, H. Botha, J. Graff-Radford, L. R. Barnard, J. L. Gunter, C. G. Schwarz et al., "Deep learning-based brain age prediction in normal aging and dementia," *Nature aging*, vol. 2, no. 5, pp. 412–424, 2022.